Liquid Jet Blasting Using Ultra-High Frequency Supersonic Pulsed Air Jet

John T. Solomon

Tuskegee University, Tuskegee, AL, USA
Email: johnts77@gmail.com

Abstract

This paper reports an experimental study on a liquid injector assembly integrated with an ultra-high frequency pulsed air jet that operates at 21 kHz. The active air-blasting assembly steadily injects a liquid through four micro-nozzles of 0.4 mm diameters each, positioned around a 1 mm nozzle through which the pulsed actuation jet flows out at supersonic velocity. High-frequency compressible air vortexes and shock waves generated by the injector atomize the liquid stream into finer droplets and distribute them to a larger area to improve mixing with the ambiance. The paper presents the design details and preliminary studies on the flow field characteristics of this novel injection scheme, which is a potential candidate for high-speed flow mixing and control applications.

Keywords

Ultrasonic Actuators, Flow Control, Liquid Blasting

1. Introduction

Effective atomization of a liquid jet and its mixing with an oxidizer are crucial steps in the efficient and stable operation of high-speed two-phase flow combustion systems such as a rocket or a scramjet engine. A coaxial injector design, in which a liquid fuel injects through a nozzle surrounded by an annular air jet, is a classical air-blasting configuration used for atomizing liquid oxygen using a high-speed gaseous hydrogen jet [1]. Although the flow dynamics of jet breakup and atomization is a very complex process, the flame stability, combustion efficiency, and emissions are closely related to the droplet mixing and its spatial density distribution [2] [3]. Several researchers explored this problem and studied the influence of liquid and gaseous jets' instabilities on droplet size and dis-

tribution [4]. Air-blasting atomization has two mechanics involved –a primary disintegration near the nozzle tip and a secondary break up far downstream. The shear force in the liquid-air boundary is responsible for the primary breakup, which is characterized by the primary breakup length that usually extends to a few diameters of the liquid jet [5] [6] [7] [8] [9]. The droplet disintegration largely depends on the relative velocity of gas and injected liquid, injector geometry, and fluid properties [10] [11]. Inertia and viscous force play critical roles in droplet formation and distribution in high-speed flows [12] [13].

The air-blasting process is inherently unsteady, and the primary breakup usually correlates to the shear instabilities and high shear forces in the liquid-air interface [14] [15]. The droplet formation downstream connects to the turbulent motion of secondary air and resulting deformation forces and its intensity. Classical studies show that viscosity plays a crucial role in drop disintegration [16]. For Low-velocity problems, Kevin Helmholtz's instabilities play a significant role, and non-dimensional parameters such as weber number and Reynold number decide the instabilities and final break up [17] [18]. Kelvin-Helmholtz, capillarity, and helical instabilities interact, resulting in the formation of complex waves in the liquid-gas interface that essentially leads to the breaking of the jet [19]. Some studies also report that jet speed and instability wave frequency have correlations to the breakup and droplet formation [20]. Several researchers studied this problem using flow visualization techniques in the past. Studies show that the gas momentum flux should be larger or equal to the liquid momentum per unit volume for effective interaction between the jets. The surface tension of liquid also played a vital role in the droplet formation and distribution by affecting the amplification of perturbations in the injected stream [21] [22].

High-speed flow mixing is a microscopic, molecular-level diffusion problem that directly connects to the atomization of the fuel jet and its interaction with the incoming high-speed air molecules. However, the macroscopic phenomena resulting from the shear layer instabilities of the mixing fluids play a significant role in the overall efficiency of the process—especially in air-breathing hypersonic flight systems. The passive fuel injection techniques use flush mounted or intrusive injectors to generate streamwise counter-rotating vortices for rapid nearfield mixing of the incoming air and fuel [23]-[29]. Beyond the classical passive coaxial configuration, active schemes such as powered resonance tubes (PRT) or Hartmann-Sprenger tubes have been explored for air-blasting atomization in the past that can provide pulsed actuation up to 15 kHz. Studies show that such active jet modulation is promising for improving penetration and high-speed mixing compared to unmodulated jets. However, the limited operational bandwidth and larger size restrict their implementation in practical systems [30]. Innovative fuel-air mixing technologies are essential to advancing next-generation air-breathing hypersonic flight systems, which are at the forefront of national priorities in defense.

2. Experimental Details

2.1. Facility Description

The current paper presents the design and experimental studies on a novel air-liquid jet injector configuration, as shown in Figure 1, that could tailor instabilities and atomize an injected fluid using a supersonic pulsed air jet blasting at an ultrasonic frequency of 21 kHz. The experiments presented in this paper were conducted in the flow diagnostic laboratory at Tuskegee University. Initial findings from this study were presented at the AIAA conference held in Orlando, FL, in 2020 [31].

The injector system shown in Figure 1 has four micro-nozzles, each 400-micrometer diameter integrated symmetrically around a 1 mm steel tube. The four micro nozzles inject a fluid inclined 30˚ to the central steel tube from which pulsed air jets flow out and atomize the injected stream of liquid. Figure 1(a) is a sectional view, and Figure 1(b) is the bottom view of the injector. Section 2 discusses more details of this pulsed air-liquid jet injector assembly and the mechanism of generating ultra-sonic supersonic pulsed jet. Figure 2 shows representative flow patterns of flowfield when the assembly injects 1) liquid stream alone at a given pressure, 2) pulsed jet alone operating at 21 kHz, and 3) pulsed jet operating at 21 kHz atomizes the liquid stream injected. This paper reports the design details of such an injector assembly and its flowfield characterization compared to a particular case, where the air jet operates in a steady injection mode without pulsing action.

Figure 3 shows a schematic of the experimental setup. The experiment uses a vibration-free optical table equipped with state-of-the-art data acquisition and flow imaging systems. A lens-based microschlieren system, as shown in Figure 4, has been set up on the optical table for visualizing the microscale flowfield of the active injector assembly. A Photron mini™ UX100 high-speed camera has been used for image acquisition. This monochromatic camera captures up to 4000 frames per second at its full resolution of 1028×1028 pixels. The microschlieren system uses a customized LED light source that provides a white light having a pulse width of 80 *ns*. Such a light source with an extremely short pulse duration allows us to "freeze" and capture the high-speed microscale flow structures in the flowfield. In the microschlieren system, the light from the LED is focused onto a sharp rectangular aperture using a condensing lens. This light is then collimated and focused on a sharp knife edge. The injector flow is kept in test section 5, as indicated in Figure 3. This system uses 60 mm lenses with a 60 mm focal length for collimating and condensing purposes. The pulsing frequency of the air jet is measured using a B&K microphone and amplifier. The signal from the microphone is amplified and filtered using an SR645 duel pass filter before it is used for generating pulsed square waves CD and AB with an appropriate delay between the pulses. These signals are then used for triggering the camera and the LED light source. High pressure compressed nitrogen tank (2000 psi or 13.8 MPa) supplies air to the pulsed jet injector assembly. As shown in

Figure 3, water from a pressurized container provides a liquid stream for the airblast experiments. 3.

2.2. Design Details of the REM-Nozzle Assembly

Figure 5(a) shows the schematic of the pulsed air-liquid stream injector assembly developed for the current experiments. This design allows the pulsed air jet from a 1 mm nozzle at the bottom of the injector block to interact with a steadily injected fluid from four 400 micrometer diameters nozzles. The present experiments use water as injected fluid. The injector assembly is fabricated with three
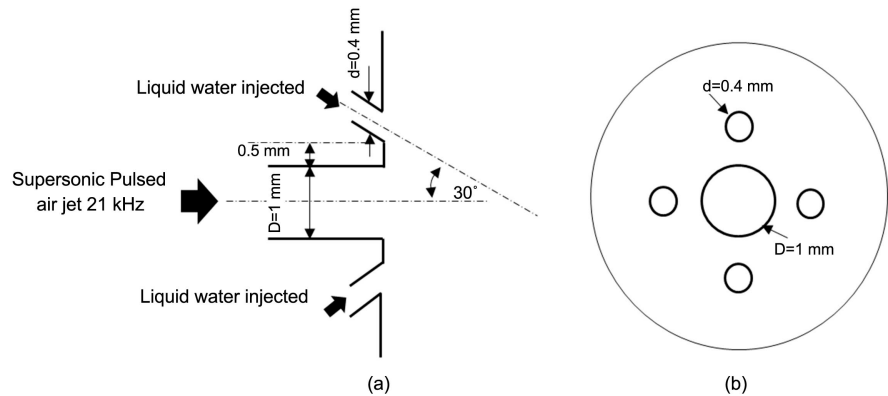
Figure 1. Schematic of pulsed air-liquid injector used for airblast atomization in this study (a) cross-sectional view (b) bottom view.
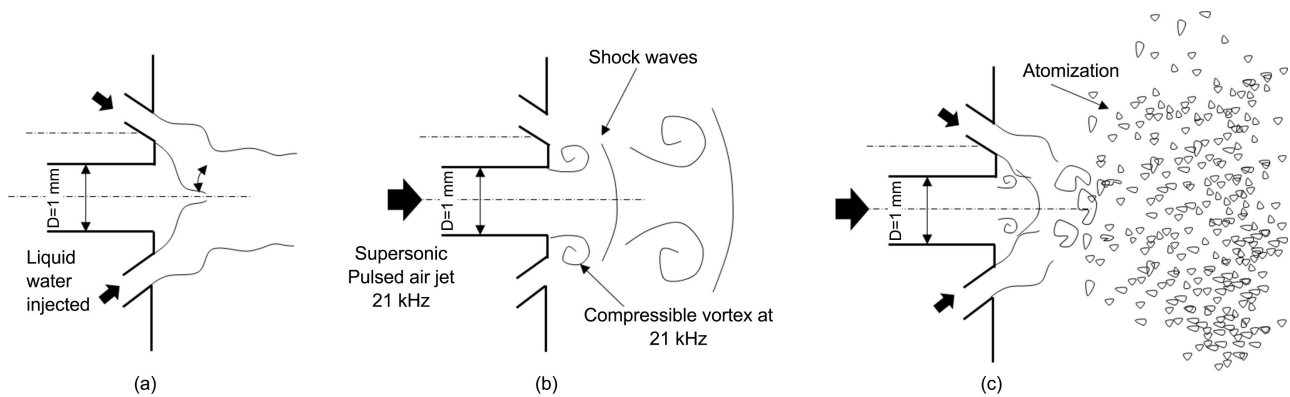

Figure 2. Flow patterns of (a) injected liquid stream, (b) pulsed air jet, and (c) pulsed airblast atomization.
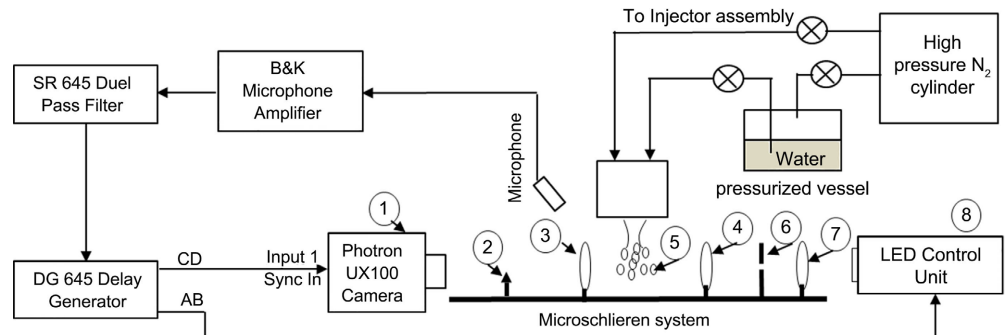

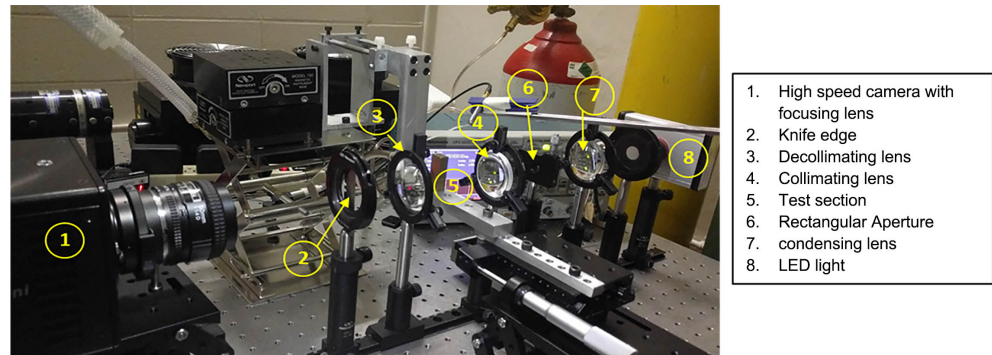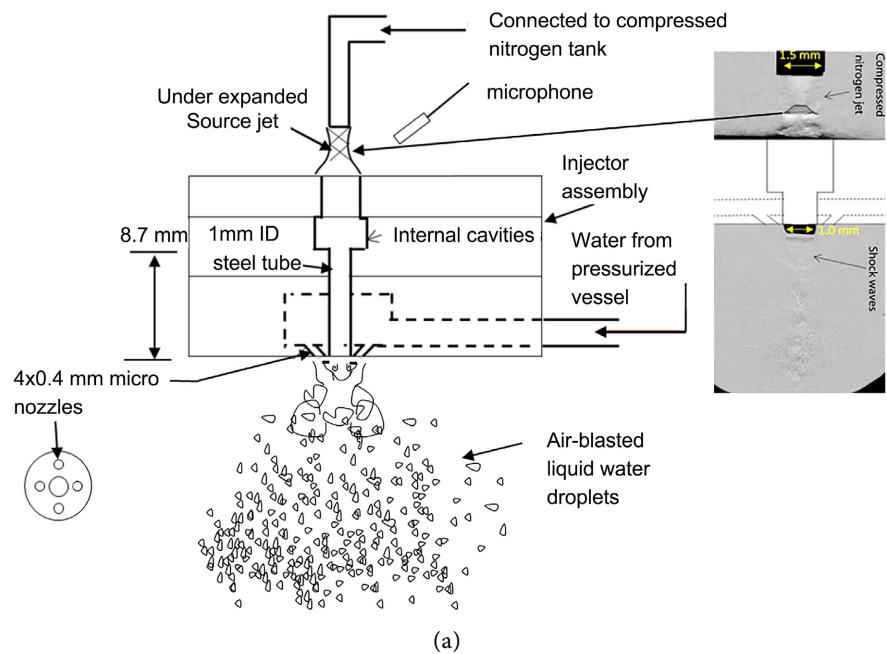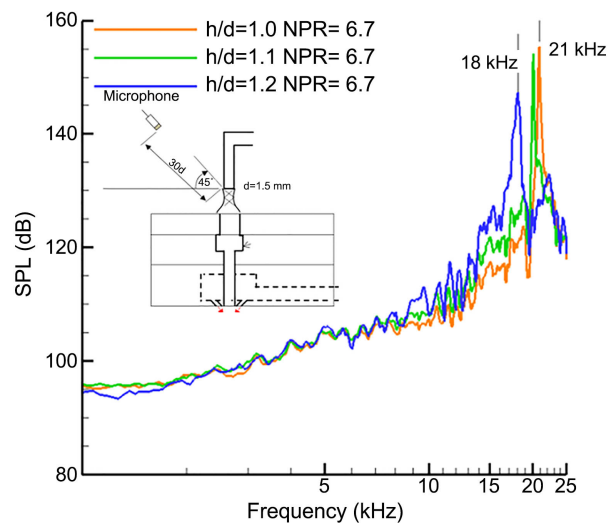**Figure 3.** Experimental setup used for the present study.

Figure 4. Microschlieren imaging set up used for flowfield visualization.

1. High speed camera with focusing lens
2. Knife edge
3. Decollimating lens
4. Collimating lens
5. Test section
6. Rectangular Aperture
7. condensing lens
8. LED light

(a)

(b)

Figure 5. (a) Schematic of a REM-Nozzle assembly used in this study; (b) Frequency characterization.

separate brass plates, as indicated in Figure 5(a). The top plate contains a 3 mm long, 1.3 mm diameter cavity through which an under-expanded source jet enters the injector assembly. The second plate has two internal cavities, and the last plate contains a fluid conduit connected to the four micronozzles. A steel tube of 1 mm diameter connects plates 2 and 3, as shown in the figure through which pulsed air jet flows out the injector.

All three plates were assembled without air or water leaks. This assembly has a total internal cavity volume of 20.6 mm^3. An under-expanded jet supplied from a source nozzle flows into the injector, fills the internal cavities, and exits through the 1 mm steel tube. This source jet entering the nozzle block produces pulsed flow through the 1 mm steel tube under suitable resonance conditions. The micro nozzles that inject the fluid were machined at an angle of 30° from the central axis. The steel tube used inside the injector assembly has a design length of 8.7 mm. The source nozzle is a steel tube of 1.5 mm in diameter. The stagnation pressure ratio upstream of this nozzle to the backpressure (atmospheric pressure) is defined as the nozzle pressure ratio *NPR*. Since the *NPR* chosen is 6.7, the degree of expansion is intense, and a Mach disc appears in the source jet, as indicated in Figure 5. The flow past the Mach disc is subsonic, which also forms part of the first shock cell of the source jet. However, when this highly under-expanded source jet flows into the cavity, it creates a "filling and discharging phenomena," producing an oscillating pressure field within the cavity. This highly oscillating pressure drives the actuation jet from the 1 mm nozzle providing low subsonic to supersonic velocity variation for the actuator jet as reported in our previous studies [32] [33]. Although the wall friction has some influence at these scales, the pressure drop across the 1 mm steel nozzle is minimal compared to the magnitude of pressure fluctuation experienced by the cavity. Our previous measurements show that the pressure fluctuation within the cavity ranges from 13 - 32 psi [33]. Since the pressure drop calculated is an order of magnitude less than the minima of this fluctuation (less than 1.3 psi), the effects of wall friction from the nozzle can be neglected. The water jet supply to the injector micronozzles while the air jet is in pulsing mode results in pulsed, airblast atomization, and entrainment of liquid droplets in the compressible vortex generated by the pulsing jet.

The state of the source jet strongly influences the pulsing phenomena and the frequency. The source jet requires some degree of under-expansion for the resonance (pulsing) phenomena to occur, defined by the parameter *NPR*. Key parameters that influence the pulsing frequency are the cavity volume of the injector assembly (*V*), nozzle pressure ratio (*NPR*), the distance between the source nozzle exit to injector entrance (*h*). In this study, the *V* and *NPR* are kept constant, and *h* is varied for adjusting (fine-tuning the pulsing frequency). Our previous studies report a parametric design equation that predicts pulsing frequency derived from a lumped element model [34] [35] [36]. Figure 5(b) shows the frequency spectra of pulsed jet measured using a microphone. In this design, the

frequency of the pulsed jet can be varied from 18 to 21 kHz by changing h/d from 1.0 to 1.2 for a constant nozzle pressure ratio of the source jet (NPR) = 6.7. The parameter d is the source nozzle diameter. The top and bottom views of the REM nozzle assembly are shown in Figure 6. More details of this injector assembly and actuator design principles are available in Solomon *et al.* [37].

3. Results and Discussions

3.1. Instantaneous Flowfield

This section presents the instantaneous flow features of the injector when water is used as an injected stream, and compressed air is used for generating the ultra-high frequency pulsed jet. The lens-based microschlieren imaging system shown in Figure 4 is used for flow visualization. The goal is to understand the airblast atomization characteristics when the injected liquid stream encounters the ultrasonic air-jet positioned at the center of the assembly. Additionally, this flowfield is compared against a particular case—in which an air jet is used in a steady injection mode without activating the induced resonance in the injector assembly. Figure 7 and Figure 8 show the baseline flow patterns of steady and pulsed injection mode without a water stream. Only the flowfield at the bottom side of the injector assembly, which is the region of interest, is presented in these images. Figures 7(a)-(c) show the instantaneous air-jet images when used in the steady mode. The figure shows an under-expanded supersonic jet steadily flowing out from the nozzle located at the center of the injector assembly. Figures 8(a)-(c) show various phases of the pulsed injection mode of air-jet without liquid injection. Figure 8(d) shows the beginning phase of the pulsing where a compressible vortex appears near the nozzle exit. The pulsing frequency is measured at 21 kHz, and section B discusses the details of this microphone measurement. Figures 8(a)-(c) show different stages of pulsed vortex evolution.
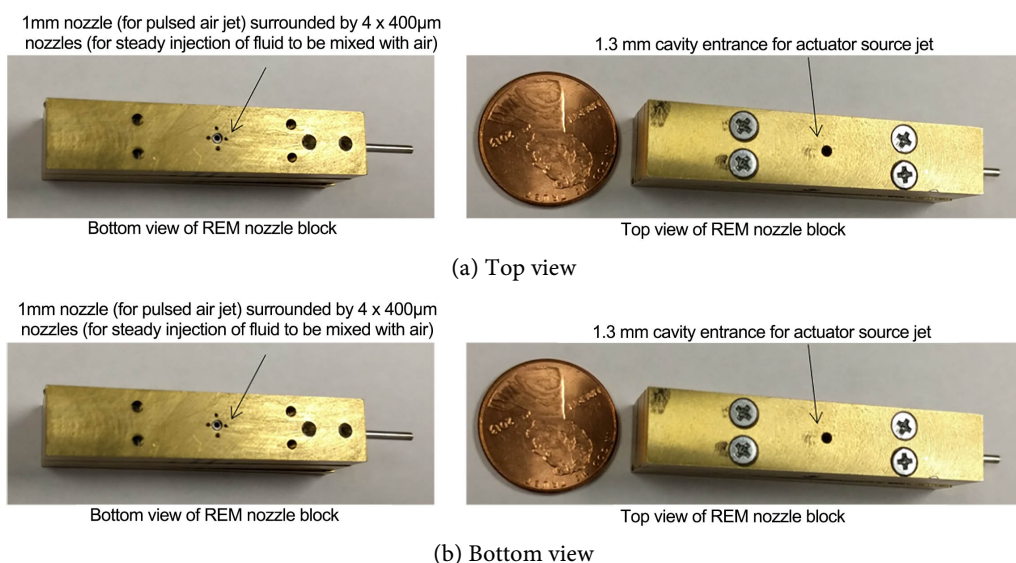

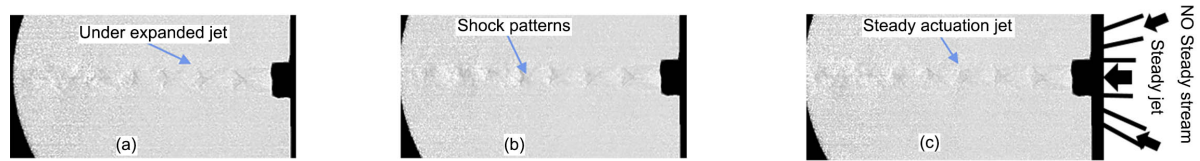**Figure 6.** Photograph of REM-Nozzle Block Design I (a) Top view (b) The bottom view.

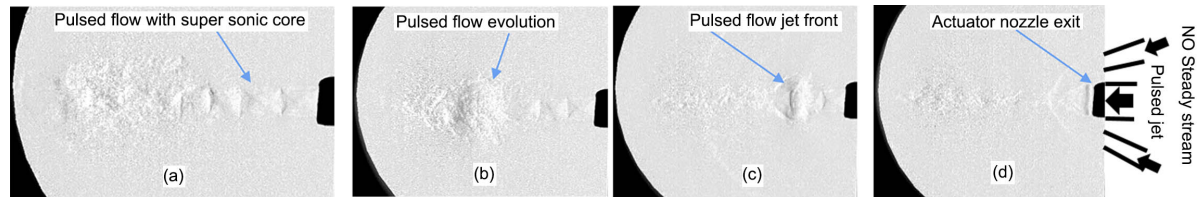**Figure 7.** Instantaneous images of steady actuation jet without injected stream.

Figure 8. Instantaneous images of pulsed actuation jet without injected stream.

These images indicate that the injector assembly generates a supersonic pulsed jet and produces a compressible vortex close to the four micronozzles used for the liquid stream injection. Our previous study shows that these vortex structures move with a velocity of 200 m/sec [31]. **Figures 9(a)-(c)** show three instantaneous images of the stream of water injected at a pressure of 5 psi (34.5 kPa) without air-jet activation. As indicated in **Figure 9(a)**, the water jets from the four micronozzles inclined at an angle of 60° merge and form a single jet at this pressure. This jet has irregular and asymmetric boundaries due to the merging of multiple instability waves from the four injected streams.

Figures 10(a)-(c) show three instantaneous images of air-jet blasting of the water stream at 5 psi (34.5 kPa) using the steady actuation jet. Air blasting of injected stream results in the dispersion of water jet to fine droplets due to the intensive shear force generated by the actuation jet. Visual inspection shows that blast generates a plume of water droplets in a conical shape with an included angle of nearly 65°. **Figure 10(a)** shows the air jet at 65 psi (448.2 kPa) surrounded by an injected stream from four micronozzles. **Figure 10(b)** indicates the location of these jets from 400-micrometer nozzles. The position of the 1 mm nozzle exit relative to the injected stream is marked in **Figure 10(c)**. Qualitative visual inspection of the instantaneous images indicates that they are very similar from one frame to another. **Figures 10(a)-(c)** show instantaneous images of the pulsed air jet blasting of the water stream at 21 kHz. The pulsed jet actuation results in the dispersion of fluid droplets to a wider angle (almost 360°) in the flowfield. From the visual comparison of instantaneous images shown in **Figure 10** and **Figure 11** (steady and pulsed actuation), it is evident that pulsed actuation results in highly dispersed droplets in the injected domain. To better understand steady and pulsed actuation dispersion characteristics on the liquid stream injection, the contour maps of two sample instantaneous flowfield images, shown in **Figure 10** and **Figure 11**, are plotted in **Figure 12**. The contour maps, which qualitatively represent the droplet dispersion and size, also indicate that pulsed actuation results in a more scattered distribution of the injected stream of fluid. Contour maps of several instantaneous images were analyzed, and they all

show very similar dispersion characteristics, as shown in **Figure 12**.

The scattered dispersion of droplets shown in **Figure 11** and pulsed flow patterns of the actuation jet shown in **Figure 8** are correlated. The high-frequency compressible vortex generated due to the pulsing action forms a spherical shock front that disintegrates the injected fluid to a wider angle and in all directions. To understand this phenomenon, the temporal flow features of the disintegrated droplets were captured at a higher frame of 64 kHz by reducing the field of view to 1280 × 72 pixel resolution. The field of view chosen for the temporal study is indicated as a red rectangular area in **Figure 11(a)**.
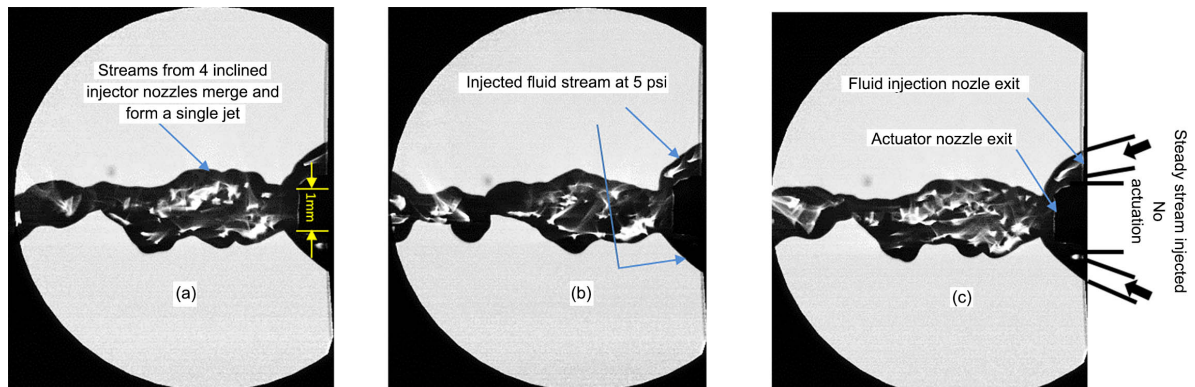

Figure 9. Instantaneous images of the injected stream at 5 psi (34.5 kPa) with no actuation air-jet.
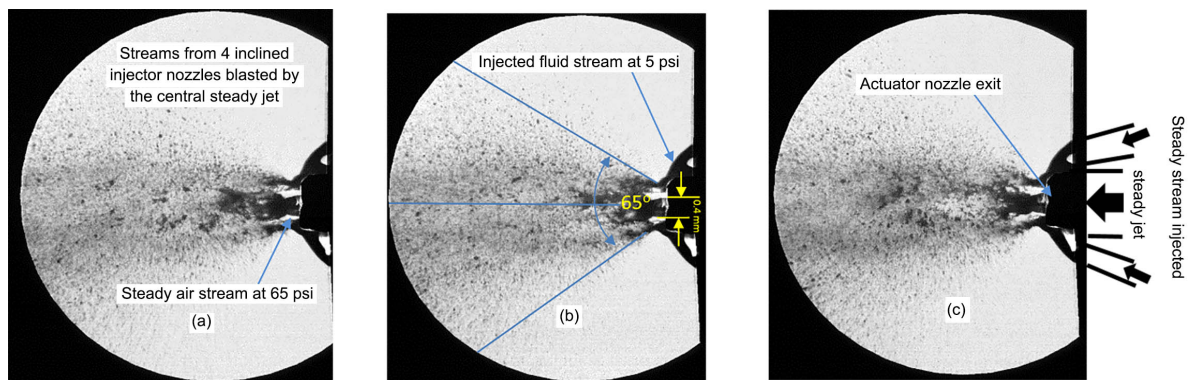

Figure 10. Instantaneous images of the injected stream with steady air jet (no pulsing) at the center.
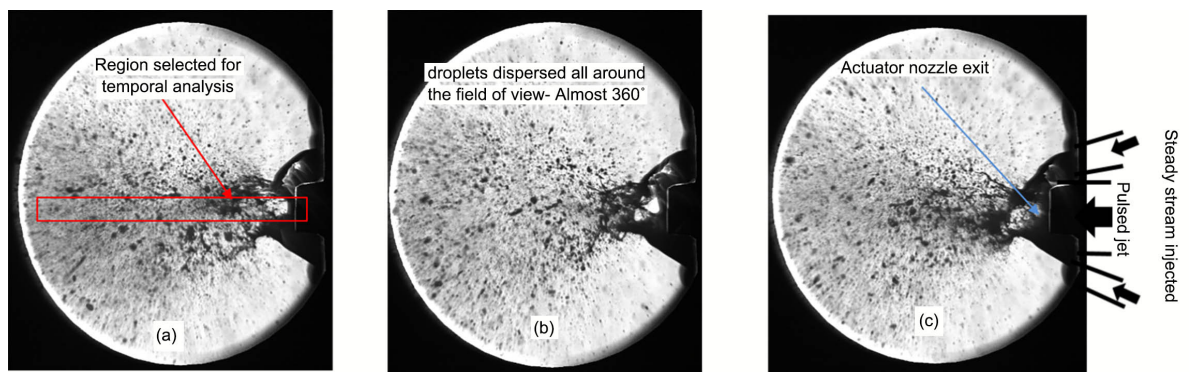

Figure 11. Instantaneous images of pulsed air blast through the central nozzle at 21 kHz frequency.
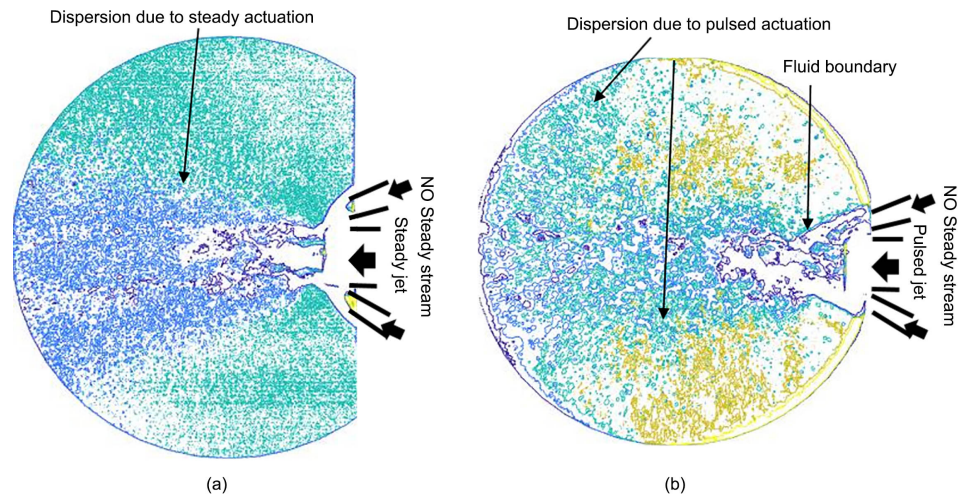
Figure 12. Contour maps of instantaneous images of pulsed and steady configurations.

3.2. Temporal Characteristics of Pulsed Air-Jet Blast

Figure 13 shows the microphone spectra of the injector assembly when air jet is used in pulsed and a steady mode of operation. The microphone is kept 45 mm away from the source jet at an angle of 45°, as indicated in Figure 5(b). The spectra measured in the nearfield show high amplitude pressure fluctuations at 21 kHz that is generated by the resonating source jet associated with the injector assembly. The spectra measured during the steady mode of operation only show broadband noise, and it picks up some low amplitude, low-frequency content from the steady air jet flow.

Figure 14 shows the image analysis procedure used to understand the temporal properties of the injector flowfield when it is in pulsed actuation mode. Figure 14(a) shows a full resolution (1028 × 1028) instantaneous image captured at a 4 kHz frame rate. A region shown inside a red rectangle is used for the temporal image analysis. These images are acquired with a frame rate of 64 kHz at a reduced resolution of 1028 × 72. Figure 14(b) shows a sample of six temporal images with a 15.625-microsecond interval. A total of 2000 continuous images were used for this analysis. As indicated in the red box in Figure 14(b), four pixels in each temporal image in a smaller region close to the actuation nozzle are stacked, as shown in Figure 14(c). The dark region indicates the presence of a liquid droplet or liquid streak in the image at a given instant of time. The intensity variation of a pixel at a given spatial location is correlated to the motion of liquid through it. Stacking these pixels for 2000 images will provide a temporal signature of the liquid motion through that region defined by the pixel intensity. The black and white band of pixel intensity map generated in this manner represents a timestamp of the effect of pulsed flow on injected fluid at a selected location of interest.

Welch power spectral density estimate is used to analyze the frequency content of this image data generated by stacking pixels. Each row of the pixel intensity map shown in Figure 14(c) contains the intensity values at a given location

for 2000 time steps. **Figure 15(a)** & **Figure 15(b)** show the power spectral density calculated for two such rows. Both power spectra show a peak at 21 kHz with a slightly different amplitude, which indicates that the pixel location selected for the analysis experience a periodic phenomenon caused by the pulsed actuation whose frequency is captured separately by a microphone. These estimates, microphone data (**Figure 13**), and using image analysis (**Figure 15**) indicate the same frequency, which means that the injected stream of liquid jets is blasted and atomized with an actuation jet operating in an ultra-high frequency of 21 kHz.
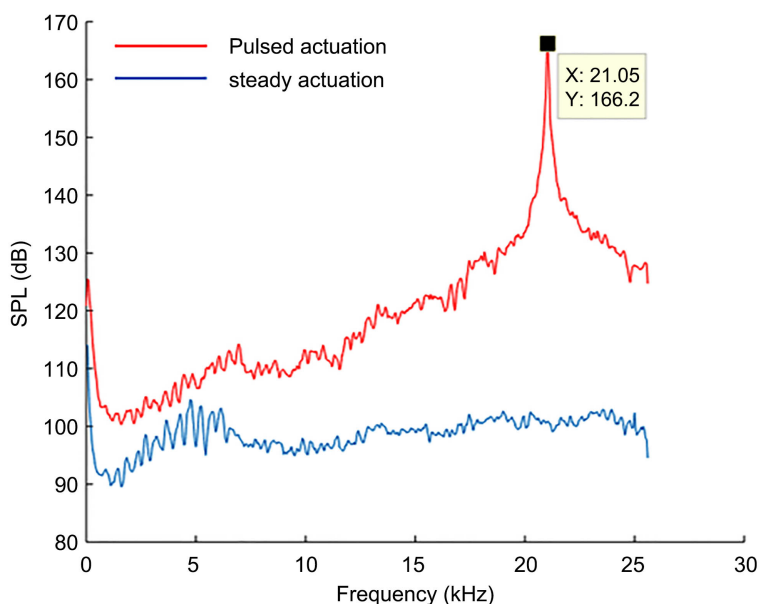

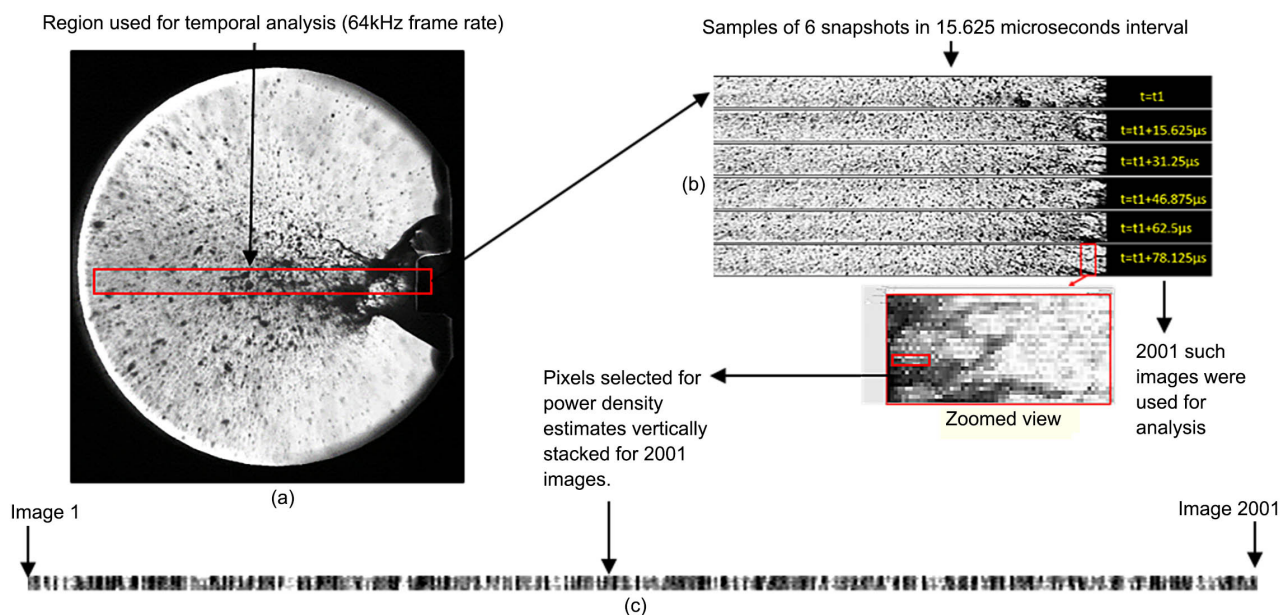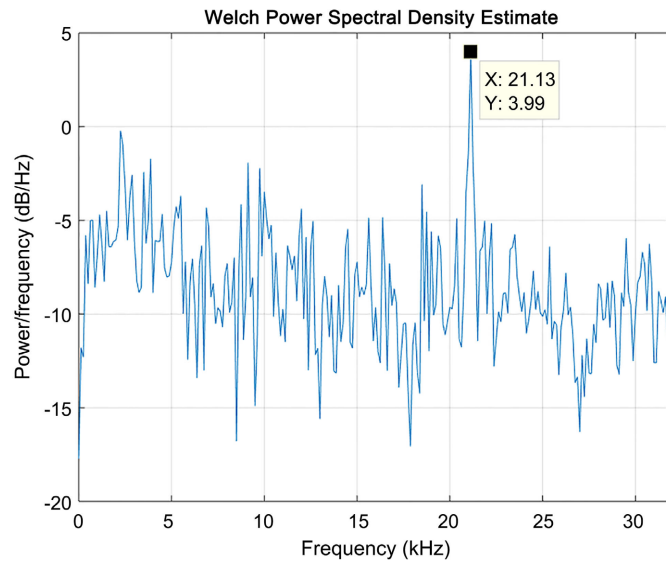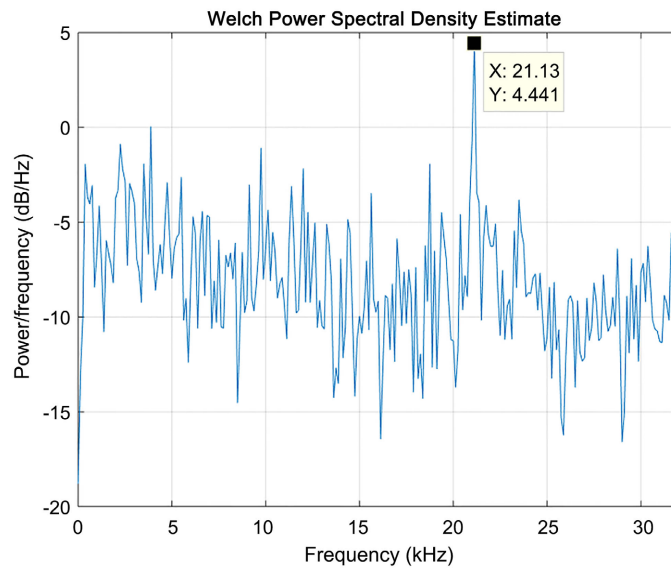**Figure 13.** Microphone spectra of pulsed and steady jet actuation.

Figure 14. Procedure used for image analysis of pulsed REM nozzle flowfield.

(a)

(b)

Figure 15. Welch power density estimate of two rows of image data shown in **Figure 14(c)**.

    The physical meaning of this power spectral density estimate of pixel intensity shown in **Figure 15** is that fluid periodically appears in a selected location which has a period of 21 kHz in that location. When fluid passes randomly through this location, it manifests as broadband noise in the power density spectra of the pixel intensity. **Figure 16** shows a stack of pixels generated using a similar temporal analysis procedure for the steady actuation mode. As mentioned earlier, this black and white image band contains temporal flow characteristics at a given spatial location. **Figure 17(a)** & **Figure 17(b)** show Welch power density spectra estimated for the intensity of this image for two rows, which is characterized only by broadband random fluctuation without any high amplitude frequency

content. Microphone data are shown in **Figure 13** also support this spectral estimate from the image analysis.

3.3. Pulsed and Steady Blast Atomization-Qualitative Comparison Using Image Analysis

To better compare the flowfield of pulsed and steady air blast of injected fluid, a sample image from each of these configurations is analyzed using imageJ™ software and Matlab™. **Figure 18(a)** shows an image of liquid injection with
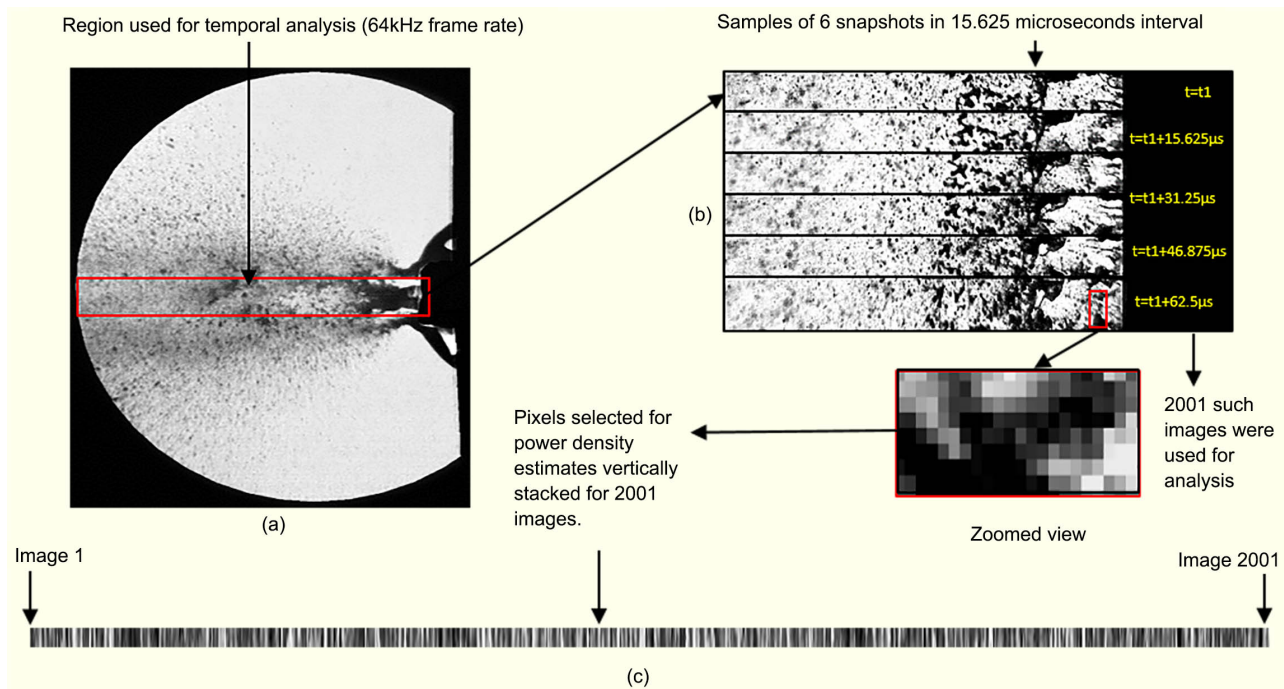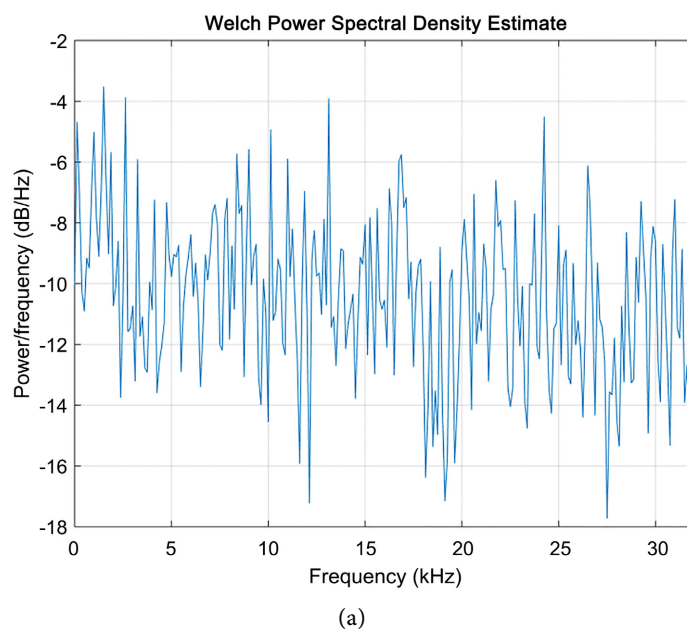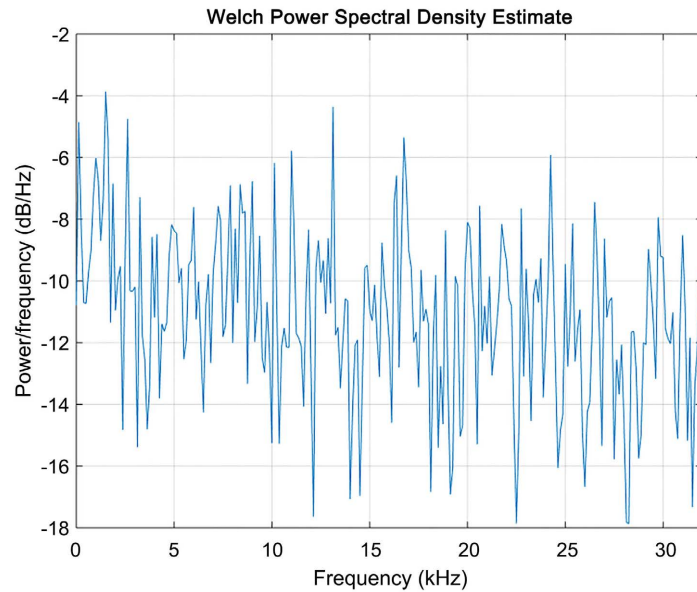

Figure 16. Pixels stacked vertically for steady jet-liquid stream injection.

(a)

(b)

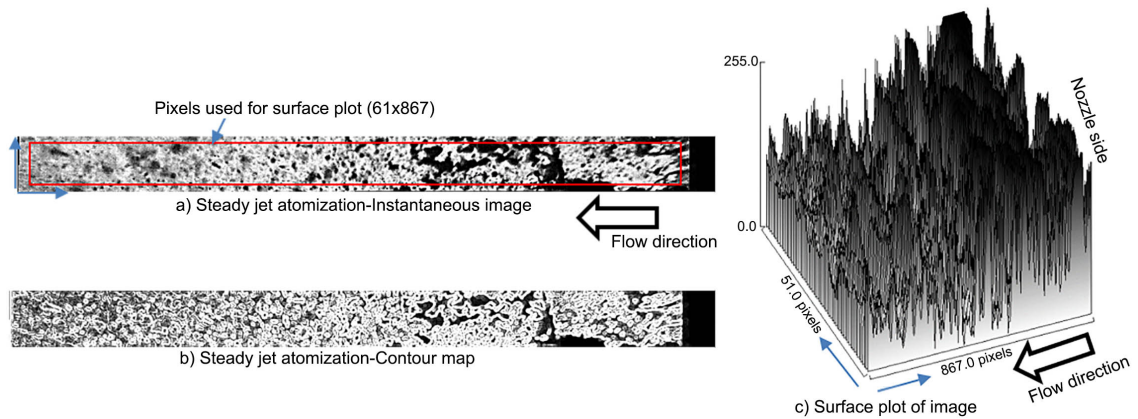**Figure 17.** Welch power density estimate of two rows of image data shown in **Figure 16**.

Figure 18. Steady jet atomization-contour map and surface plot.

steady actuation, and **Figure 18(b)** represents its contour map. The contour map provides qualitative information on the droplet size and distribution for a given instantaneous image at the specified location. **Figure 16(c)** shows the surface plot of the same image by trimming the edges to 61×866 pixel size. The intensity of pixels in horizontal and vertical directions in this two-dimensional image essentially correlates to the presence of a liquid droplet and its relative distribution and size. Larger streaks of liquid seen near the nozzle exit (**Figure 18(a)**) is characterized by darker and broad peaks and region away from the nozzle captured by fine discrete peaks, which indicate distinctive droplet dispersion in that region. Sharp and discrete peaks correspond to smaller droplets, while thicker and broad peaks indicate larger droplets and liquid streaks in the flow.

Figures 19(a)-(c) show a similar contour and surface plots for liquid stream

injection with pulsed actuation of 21 kHz. A closer look at **Figure 19(b)** & **Figure 19(c)** indicates that pulsed actuation generates droplets with a smaller size as the surface plot contains more discrete and sharper peaks than the previous case.

3.4. Pulsed and Steady Blast Atomization-Particle Velocity Estimate

Image analysis in **Figure 18** and **Figure 19** shows distinctive and qualitative features for steady and pulsed jet actuation on the liquid stream injected through this active nozzle assembly. The temporal images captured at 64 kHz are used to estimate droplet speed fluctuation during the pulsing phase. **Figure 20** shows a stack of six continuous images taken at 15.625-microsecond intervals for this purpose. These images contain signatures of pulsed liquid stream ejection. Marked in red circles, set 1 contains 5 temporal images that carry traces of a pulsing streak of liquid and its disintegration into droplets.

In Set 1, the first image is the beginning phase of the pulsed ejection. The movement of a liquid streak for 62.5 microseconds is estimated as 3.9 mm, which gives a velocity of ~63 m/sec for the blasting liquid jet. Our previous experiments indicated that the pulsed vortex moves with a speed of 200 m/sec [31] when a gas is used as an injected stream, and liquid injection slows down this speed by nearly 30%. Another set of tracked particles is marked in blue circles away from the pulsing stream of fluid particles. The particles tracked in Set 2 have a different speed which is estimated as ~25 m/sec. The cyclic speed variation of the pulsing jet is responsible for the speed fluctuation in the injected stream. Other than these speed estimates, other particle motion is also observed from these images. For example, in Set 3 (the green circle and line), particle motion shows a different space-time slope indicating a different speed than Set 1 and 2.

Figure 21 shows a similar particle speed estimate for the injected stream with steady actuation. In this case, the motion identified for the injected stream indicated in red circles shows a speed of 25 m/sec. Unlike the patterns seen in **Figure 19**, steady actuation results in liquid droplets moving relatively at a constant speed.
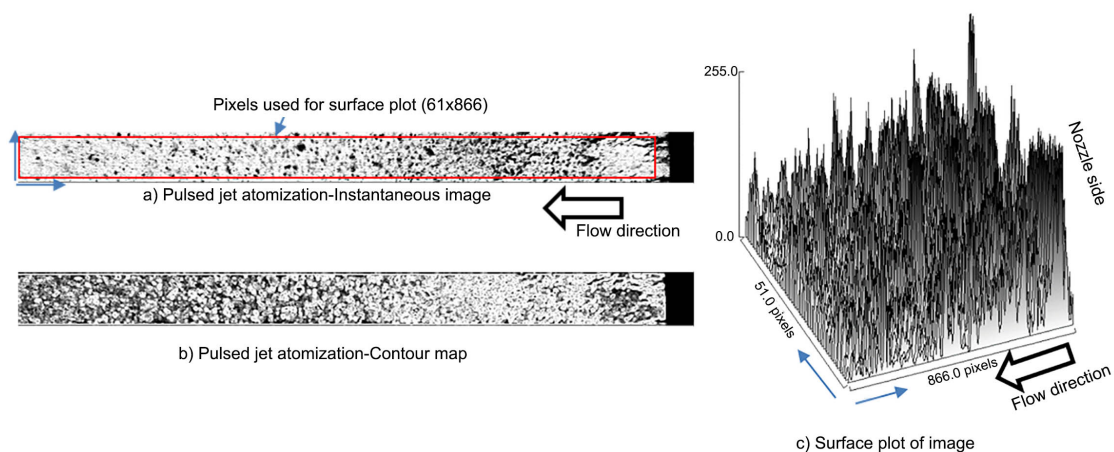

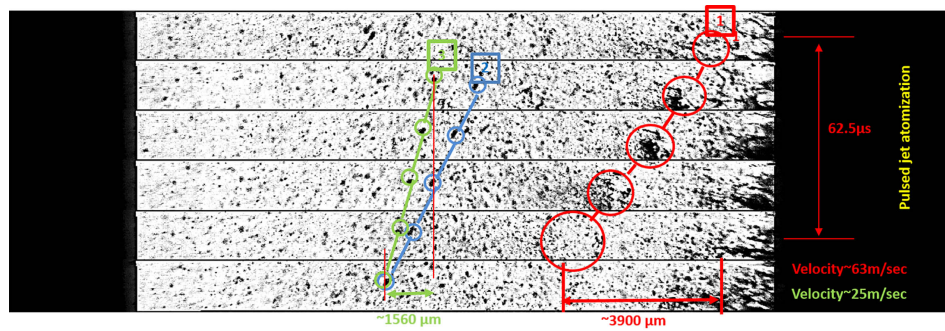**Figure 19.** Pulsed jet atomization-contour map and surface plot.

Figure 20. Speed estimation from temporal images of Pulsed injection.
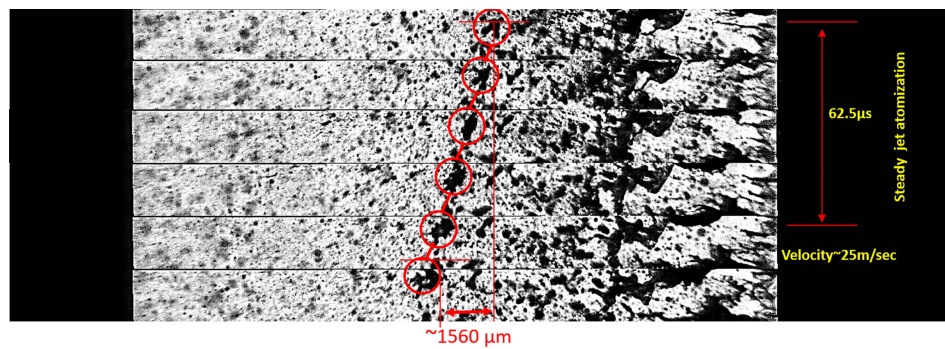

Figure 21. Speed estimation from temporal images of steady injection.

4. Summary and Future Work

An experimental study on an active liquid jet injection assembly integrated with an ultra-high frequency pulsed air jet is reported in this paper. The active nozzle assembly steadily injects a fluid (liquid water) through four micro-nozzles of 400 µm diameter positioned around a 1 mm nozzle through which supersonic actuation air-jet flows out at 21 kHz frequency. The pulsed air jet develops a high-frequency compressible air vortex in the injected flowfield and ensures air-blast atomization and entrainment of the liquid jet injected through the micro-nozzles. Image analysis indicates that ultra-high frequency pulsed actuation mode generates finer droplets and broader distribution than steady air blasting from the same injector under similar conditions. Microschlieren temporal images acquired at a 64 kHz frame rate are used for particle speed estimation and other qualitative characteristics of the injected stream. In the future, PIV and PLIF techniques will be used to study the quantitative mixing characteristics of this nozzle assembly.

Acknowledgements

Conflicts of Interest

The author declares no conflicts of interest regarding the publication of this paper.

References

[1] Burick, R.J. (1972) Space Storable Propellant Performance Program Coaxial Injectors Characterization. NASA-CR-120936.

[2] Lefevvre, A.H. (1989) Atomization and Sprays. Tailor and Francis CRC Press, Boca Raton. https://doi.org/10.1201/9781482227857

[3] Gomi, H. (1985) Pneumatic Atomization with Coaxial Injectors: Measurements of Drop Sizes by the Diffraction Method and Liquid Phase Fraction by the Attenuation Method of Light. NAL-TR-888T, N 86-27595.

[4] Hoyt, J.W. and Tailor, J.J. (1977) Waves on Water Jets. *Journal of Fluid Mechanics*, **83**, 119-127. https://doi.org/10.1017/S0022112077001074

[5] Lasheras, J.C., Villermaux, E.V. and Hopfinger, E.J. (1998) Breakup and Atomization of a Round Water Jet by a High-Speed Annular Air Jet. *Journal of Fluid Mechanics*, **357**, 351-379. https://doi.org/10.1017/S0022112097008070

[6] Eroglu, H., Chigier, N. and Farago, Z. (1991) Coaxial Atomizer Liquid Intact Lengths. *Physics of Fluids*, **3**, 303-308. https://doi.org/10.1063/1.858139

[7] Engelbert, C., Hardalupas, Y. and Whitelaw, J.H. (1995) Breakup Phenomena in Coaxial Airblast Atomizers. *Proceedings of the Royal Society of London*, *Series A, Mathematical, Physical and Engineering Sciences*, **451**, 189-229. https://doi.org/10.1098/rspa.1995.0123

[8] Lin, S. and Reitz, R. (1998) Drop and Spray Formation from a Liquid Jet. *Annual Review of Fluid Mechanics*, **30**, 85-105. https://doi.org/10.1146/annurev.fluid.30.1.85

[9] Abhijeet, K. and Srikrishna, S. (2018) Liquid Jet Breakup Unsteadiness in a Coaxial Airblast Atomizer. *International Journal of Spray and Combustion Dynamics*, **10**, 211-230. https://doi.org/10.1177/1756827718760905

[10] Reitz, R. and Bracco, F. (1982) Mechanism of Atomization of a Liquid Jet. *The Physics of Fluids*, **25**, 1730-1742. https://doi.org/10.1063/1.863650

[11] Zhao, H., Liu, H.F., Tian, X.S., Xu, J.L., Li, W.F. amd Lin, K.F. (2014) Influence of Atomizer Exit Area Ratio on the Breakup Morphology of Coaxial Air And Round Water Jets. *AIChE Journal*, **60**, 2335-2345. https://doi.org/10.1002/aic.14414

[12] Kolmogorov, A.N. (1949) On the Disintegration of Drops by Turbulent Flows. *Doklady Akademii Nauk SSSR*, **66**, 825-828.

[13] Hinze, J.O. (1955) Fundamentals of the Hydrodynamic Mechanism of Splitting in Dispersion Processes. *AIChE Journal*, 1, 289-295. https://doi.org/10.1002/aic.690010303

[14] Chigier, N. and Farago, Z. (1992) Morphological Classification of the Disintegration of Round Liquid Jets in a Coaxial Air Stream. *Atomization Sprays*, **2**, 137-153. https://doi.org/10.1615/AtomizSpr.v2.i2.50

[15] Chigier, N. and Reitz, R.D. (1996) Regimes of Jet Breakup and Breakup Mechanisms (Physical Aspects). *Recent Advances in Spray Combustion*, **1**, 109-135. https://doi.org/10.2514/5.9781600866418.0109.0135

[16] Rayleigh, L. (1878) On the Instabilities of Jets. *Proceedings of the London Mathematical Society*, s**1**-**10**, 4-13. https://doi.org/10.1112/plms/s1-10.1.4

[17] Dombrowski, N. and Johns, W.R. (1963) The Aerodynamic Instability and Disintegration of Viscous Liquid Sheets. *Chemical Engineering Science*, **18**, 203-214. https://doi.org/10.1016/0009-2509(63)85005-8

[18] Adelburg, M. (1968) Mean Drop Size Resulting from the Injection of a Liquid Jet into a High-Speed Gas Stream. *AIAA Journal*, **6**, 1143-1147. https://doi.org/10.2514/3.4686

[19] Eroglu, H. and Chigier, N. (1991) Wave Characteristics of Liquid Jets from Airblast Coaxial Atomizers. *Atomization Sprays*, **1**, 349-366. https://doi.org/10.1615/AtomizSpr.v1.i4.10

[20] Villermaux, E., Rehab, H. and Hopfinger, E.J. (1994) Breakup Régimes and Self-Sustained Pulsations in Coaxial Jets. *Meccanica*, **29**, 393-401. https://doi.org/10.1007/BF00987574

[21] Porcheron, E., Carreau, J.L. and Le Visage, D. (2002) Effect of Injection Gas Density on Coaxial Liquid Jet Atomization. *Atomization Sprays*, **12**, 209-227. https://doi.org/10.1615/AtomizSpr.v12.i123.110

[22] Leroux, B., Delabroy, O. and Lacas, F. (2007) Experimental Study of Coaxial Atomizers Scaling. Part I: Dense Core Zone. *Atomization Sprays*, **17**, 381-407. https://doi.org/10.1615/AtomizSpr.v17.i5.10

[23] Seiner, J.M., Dash, S.M. and Kenzakowski, D.C. (2001) Historical Survey on Enhanced Mixing in Scramjet Engines. *Journal of Propulsion and Power*, **17**, 1273-1286. https://doi.org/10.2514/2.5876

[24] Gutmark, E.J., Schadow, K.C. and Yu, K.H. (1995) Mixing Enhancement in Supersonic Free Shear Flows. *Annual Review of Fluid Mechanics*, **27**, 375-417. https://doi.org/10.1146/annurev.fl.27.010195.002111

[25] Bogdanoff, D.W. (1994) Advanced Injection and Mixing Techniques for Scramjet Combustors. *Journal of Propulsion and Power*, **10**, 183-190. https://doi.org/10.2514/3.23728

[26] Drozda, T.G., Baurle, R.A. and Drummond, J.P. (2016) Impact of Flight Enthalpy, Fuel Stimulant, and Chemical Reactions on the Mixing Characteristics of Several Injectors at Hypervelocity Flow Conditions. NASA Langley Research Center, Hampton, VA, Document ID: 20160009131. https://ntrs.nasa.gov/api/citations/20160009131/downloads/20160009131.pdf

[27] Menon, S. (1989) Shock-Wave-Induced Mixing Enhancement in Scramjet Combustors. 27*th Aerospace Sciences Meeting*, Reno, NV, 9-12 January 1989, AIAA Paper 89-0104. https://doi.org/10.2514/6.1989-104

[28] Ben-Yakar, A. and Hanson, R. (2001) Cavity Flame-Holders for Ignition and Flame Stabilization in Scramjets: An Overview. *Journal of Propulsion and Power*, **17**, 869-877. https://doi.org/10.2514/2.5818

[29] Hsu, K., Carter, C.D., Gruber, M.R. and Tam, C. (2009) Mixing Study of Strut Injectors in Supersonic Flows. 45*th AIAA/ASME/SAE/ASEE Joint Propulsion Conference*, Denver, CO, 2-5 August 2009, AIAA Paper 2009-5226. https://doi.org/10.2514/6.2009-5226

[30] Gu, H.B., Li, Z., Li, F., Chen, L.H., Gu, S.L., and Chang, X.Y. (2011) Characteristics of Supersonic Combustion with Hartmann-Sprenger Tube Aided Fuel Injection. 17*th AIAA International Space Planes and Hypersonic Systems and Technologies Conference*, Francisco, CA, 11-14 April 2011, AIAA Paper 2011-2326.

[31] Solomon, J.T., Brown, K.A. and Brooks, K. (2020) Active Injection Nozzles for High-Speed Flow Mixing. *AIAA Scitech* 2020 *Forum*, Orlando, FL, 6-10 January 2020, AIAA Paper 2020-2245. https://doi.org/10.2514/6.2020-2245

[32] Uzun, A., Solomon, J.T., Foster, C.H., Oates, W.S., Hussaini, M.Y. and Alvi, F.S. (2013) Flow Physics of a Pulsed Microjet Actuator for High-Speed Flow Control. *AIAA Journal*, **51**, 2894-2918. https://doi.org/10.2514/1.J052525

[33] Solomon, J.T., Foster, C. and Alvi, F.S. (2013) Design and Characterization of High-Bandwidth, Resonance Enhanced, Pulsed Microactuators: A Parametric Study. *AIAA Journal*, **51**, 386-396. https://doi.org/10.2514/1.J051806

[34] Solomon, J.T., Cairnes, K., Nayak, C., Jones, M. and Alexander, D. (2018) Design and Characterization of Nozzle Injection Assemblies Integrated High-Frequency Microactuators. *AIAA Journal*, **56**, 3436-3448. https://doi.org/10.2514/1.J056642

[35] Ali, M.Y., Arora, N., Topolski, M., Alvi, F.S. and Solomon, J.T. (2017) Properties of Resonance Enhanced Microjets in Supersonic Crossflow. *AIAA Journal*, **55**, 1075-1081. https://doi.org/10.2514/1.J055082

[36] Solomon, J.T., Kumar, R. and Alvi, F.S. (2010) High-Bandwidth Pulsed Microactuators for High-Speed Flow Control. *AIAA Journal*, **48**, 2386-2396. https://doi.org/10.2514/1.J050405

[37] Solomon, J.T. (2010) High-Bandwidth Unsteady Actuators for Active Control of High-Speed Flows. Ph.D. Dissertation, Florida State University, Florida.